J|A|C|S ARTICLES

Published on Web 10/06/2010

Controlling Charge Separation and Recombination Rates in CdSe/ZnS Type I Core−Shell Quantum Dots by Shell Thicknesses

Haiming Zhu, Nianhui Song, and Tianquan Lian*

Department of Chemistry, Emory University, Atlanta, Georgia 30322

Received July 28, 2010; E-mail: tlian@emory.edu

Abstract: Type I core/shell quantum dots (QDs) have been shown to improve the stability and conversion efficiency of QD-sensitized solar cells compared to core only QDs. To understand how the shell thickness affects the solar cell performance, its effects on interfacial charge separation and recombination kinetics are investigated. These kinetics are measured in CdSe/ZnS type I core/shell QDs adsorbed with anthroquinone molecules (as electron acceptor) by time-resolved transient absorption spectroscopy. We show that the charge separation and recombination rates decrease exponentially with the shell thickness (d), $k(d) = k_0e^{-\beta d}$, with exponential decay factors β of 0.35 ± 0.03 per Å and 0.91 ± 0.14 per Å, respectively. Model calculations show that these trends can be attributed to the exponential decrease of the 1S electron and hole densities at the QD surface with the shell thickness. The much steeper decrease in charge recombination rate results from a larger hole effective mass (than electron) in the ZnS shell. This finding suggests possible ways of optimizing the charge separation yield and lifetime by controlling the thickness and nature of the shell materials.

Introduction

Quantum dots (QDs) have been widely explored in bioimaging,[1,2] lasing,[3] light emitting diodes,[4,5] and solar cells[6−9] because of their size dependence properties, flexible solution processing, and higher photostability compared to traditional organic dyes.[10,11] Interest in their application in solar cells has intensified in recent years,[6,9,12−20] in part because of reports of the highly controversial multiexciton generation process in these materials.[3,21−32] However, as a light harvesting component in photovoltaic devices, the stability of core only QDs remains an issue due to photoinduced oxidation.[17,18,33] It has been reported that overcoating a wide band gap shell (such as ZnS) on bare CdSe QDs to form type I core/shell structures can greatly enhance their photostability[18] and efficiency[13−16] in QD-sensitized solar cells. The ZnS shell is thought to passivate the

(1) Chan, W. C. W.; Nie, S. *Science* **1998**, *281*, 2016–2018.
(2) Bruchez, M.; Moronne, M.; Gin, P.; Weiss, S.; Alivisatos, A. P. *Science* **1998**, *281*, 2013–2016.
(3) Klimov, V. I. *J. Phys. Chem. B* **2006**, *110*, 16827–16845.
(4) Colvin, V. L.; Schlamp, M. C.; Alivisatos, A. P. *Nature* **1994**, *370*, 354–357.
(5) Steckel, J. S.; Snee, P.; Coe-Sullivan, S.; Zimmer, J. P.; Halpert, J. E.; Anikeeva, P.; Kim, L.-A.; Bulovic, V.; Bawendi, M. G. *Angew. Chem., Int. Ed.* **2006**, *45*, 5796–5799.
(6) Kamat, P. V. *J. Phys. Chem. C* **2008**, *112*, 18737–18753.
(7) Huynh, W. U.; Dittmer, J. J.; Alivisatos, A. P. *Science* **2002**, *295*, 2425–2427.
(8) Gur, I.; Fromer Neil, A.; Geier Michael, L.; Alivisatos, A. P. *Science* **2005**, *310*, 462–5.
(9) Sargent, E. H. *Nat. Photonics* **2009**, *3*, 325–331.
(10) Brus, L. E. *J. Chem. Phys.* **1984**, *80*, 4403–4409.
(11) Alivisatos, A. P. *Science* **1996**, *271*, 933–937.
(12) Robel, I.; Subramanian, V.; Kuno, M.; Kamat, P. V. *J. Am. Chem. Soc.* **2006**, *128*, 2385–2393.
(13) Shen, Q.; Kobayashi, J.; Diguna, L. J.; Toyoda, T. *J. Appl. Phys.* **2008**, *103*, 084304.
(14) Mora-Seró, I. n.; Giménez, S.; Fabregat-Santiago, F.; Gómez, R.; Shen, Q.; Toyoda, T.; Bisquert, J. *Acc. Chem. Res.* **2009**, *42*, 1848–1857.
(15) Diguna, L. J.; Shen, Q.; Kobayashi, J.; Toyoda, T. *Appl. Phys. Lett.* **2007**, *91*, 023116.
(16) Barea, E. M.; Shalom, M.; Giménez, S.; Hod, I.; Mora-Seró, I.; Zaban, A.; Bisquert, J. *J. Am. Chem. Soc.* **2010**, *132*, 6834–6839.
(17) Peng, X. G.; Schlamp, M. C.; Kadavanich, A. V.; Alivisatos, A. P. *J. Am. Chem. Soc.* **1997**, *119*, 7019.
(18) Sambur, J. B.; Parkinson, B. A. *J. Am. Chem. Soc.* **2010**, *132*, 2130–2131.
(19) Xie, R.; Kolb, U.; Li, J.; Basche, T.; Mews, A. *J. Am. Chem. Soc.* **2005**, *127*, 7480–7488.
(20) Tachibana, Y.; Akiyama, H. Y.; Ohtsuka, Y.; Torimoto, T.; Kuwabata, S. *Chem. Lett.* **2007**, *36*, 88–89.
(21) Nozik, A. J. *Phys. E (Amsterdam, Neth.)* **2002**, *14*, 115–120.
(22) Klimov, V. I. *Appl. Phys. Lett.* **2006**, *89*, 123118/1–123118/3.
(23) Schaller, R. D.; Klimov, V. I. *Phys. Rev. Lett.* **2004**, *92*, 186601–186604.
(24) Ellingson, R. J.; Beard, M. C.; Johnson, J. C.; Yu, P.; Micic, O. I.; Nozik, A. J.; Shabaev, A.; Efros, A. L. *Nano Lett.* **2005**, *5*, 865–871.
(25) Luther, J. M.; Beard, M. C.; Song, Q.; Law, M.; Ellingson, R. J.; Nozik, A. J. *Nano Lett.* **2007**, *7*, 1779–1784.
(26) Schaller, R. D.; Sykora, M.; Pietryga, J. M.; Klimov, V. I. *Nano Lett.* **2006**, *6*, 424–429.
(27) Trinh, M. T.; Houtepen, A. J.; Schins, J. M.; Hanrath, T.; Piris, J.; Knulst, W.; Goossens, A. P. L. M.; Siebbeles, L. D. A. *Nano Lett.* **2008**, *8*, 1713–1718.
(28) Nair, G.; Bawendi, M. G. *Phys. Rev. Lett.* **2007**, *76*, 081304.
(29) Pijpers, J. J. H.; Hendry, E.; Milder, M. T. W.; Fanciulli, R.; Savolainen, J.; Herek, J. L.; Vanmaekelbergh, D.; Ruhman, S.; Mocatta, D.; Oron, D.; Aharoni, A.; Banin, U.; Bonn, M. *J. Phys. Chem. C* **2007**, *111*, 4146–4152.
(30) Ben-Lulu, M.; Mocatta, D.; Bonn, M.; Banin, U.; Ruhman, S. *Nano Lett.* **2008**, *8*, 1207–1211.
(31) McGuire, J. A.; Joo, J.; Pietryga, J. M.; Schaller, R. D.; Klimov, V. I. *Acc. Chem. Res.* **2008**, *41*, 1810.
(32) Pijpers, J. J. H.; Ulbricht, R.; Tielrooij, K. J.; Osherov, A.; Golan, Y.; Delerue, C.; Allan, G.; Monn, M. *Nat. Phys.* **2009**, *5*, 811–814.
(33) Spanhel, L.; Haase, M.; Weller, H.; Henglein, A. *J. Am. Chem. Soc.* **1987**, *109*, 5649–5655.

10.1021/ja106710m

Chart 1. Photoinduced Charge Separation (k_{CS}) and Recombination (k_R) Processes in CdSe/ZnS Core/Shell QD−Anthraquinone Complexes

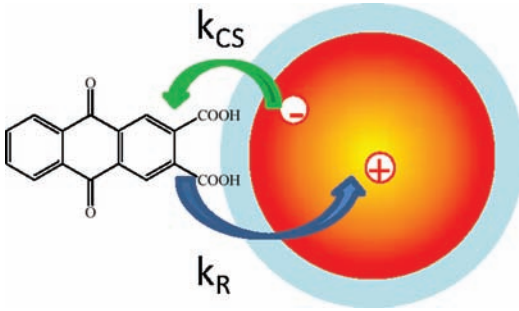

trap sites on the surface of core materials, increasing their fluorescence quantum yields.[34,35] Furthermore, it insulates the holes in the core materials, preventing their photooxidation and improving their photostability.[19,34,36] However, how the ZnS shell affects the efficiency of solar cells remains poorly understood.

In solar cells based on QD-sensitized oxide nanostructures, the incident-photon-to-current conversion efficiency depends on the efficiencies of many processes, including light harvesting, charge separation, recombination, and carrier collection.[37] The presence of the ZnS shell on the CdSe core is expected to slow down the rate of charge separation and recombination across the oxide/QD interface as well as to retard the regeneration rate of the neutral QD (from the oxidized form) by the redox mediators in the electrolyte. However, a quantitative measurement and understanding of the effects of the shell on these processes have not been achieved so far. Such quantitative understanding not only is needed for a rational optimization of the solar cell performance by controlling the shell materials and thickness but also provides an opportunity to test the theoretical models for describing charge transfer processes from and to QDs.

Here we report a study of the effect of the ZnS shell thickness on the charge separation and recombination dynamics between CdSe/ZnS type I core/shell QDs and adsorbed electron acceptors, anthraquinone-2,3-dicarboxylic acid (AQ, see Chart 1). As will be discussed later, the estimated reduction and oxidation potentials of the QDs in the 1S exciton state are −0.87 and +1.7 V (vs NHE), respectively. The reduction (oxidation) potential of AQ is −0.71 V (>+1.9 V) (vs NHE).[38,39] In this system, excitons in QDs cannot be quenched by energy transfer or hole transfer to the adsorbate. Optical excitation of QDs is expected to lead to electron transfer (ET, with rate constant k_{CS}) to AQ, and the charge separated state recombines (with rate constant k_R) to regenerate the QD and AQ ground state, as shown in eq 1:[40,41]

$$\mathrm{QD^*[1S(e),1S(h)]{-}AQ} \xrightarrow{k_{CS}} \mathrm{QD^+[h]{-}AQ^-} \xrightarrow{k_R} \mathrm{QD{-}AQ} \quad (1)$$

Here QD*[1S(e),1S(h)] is the excited QD in its 1S exciton state, $QD^+[h]$ is the oxidized QD with a hole in the valence band or trap states, and AQ^- is the reduced adsorbate. We measure the rates of charge separation and recombination as a function of the shell thickness by transient absorption spectroscopy. We show that these rates decrease exponentially with the ZnS shell thickness (d):

$$k(d) = k_0 e^{-\beta d} \quad (2)$$

where k_0 is the charge separation or recombination rate for bare QDs. However, the decay constant β for charge separation (0.35 ± 0.03 per Å) is significantly smaller than that for charge recombination (0.91 ± 0.14 per Å). We show that the observed dependence can be attributed to the decrease of the QD surface electron and hole density with the shell thickness.

Experimental Methods

Nanoparticle Synthesis. Octydecylamine (ODA) capped CdSe QDs were synthesized according to a previously published procedure.[42] Briefly, a mixture of 0.8 mmol of CdO, 3.2 mmol of stearic acid, and 12 mL of 1-octadecene (ODE) was heated to about 280 °C under N_2 protection. After CdO was dissolved, the solution was cooled to 80 °C and 3 g of ODA were added into the flask. The solution was reheated to 270 °C, to which a selenium stock solution (2 mmol of Se dissolved in 2 mL of ODE and 0.5 g of triobutylphosphine) was swiftly injected. The growth of CdSe QDs was carried out at 250 °C for 20 s. After precipitation with methanol and redissolving in hexane, the size and concentration of CdSe QDs were determined using the reported 1S exciton absorption band position and extinction coefficients of CdSe QDs.[43]

The ZnS shell was grown by a successive ion layer adsorption and reaction (SILAR) method.[42] A zinc precursor solution (0.08 M) was prepared by dissolving 0.064 g of ZnO in 2.5 mL of OA and 7 mL of ODE at 300 °C to obtain a colorless solution. The precursor solution was then maintained at above 100 °C. The sulfur injection solution (0.08 M) was prepared by dissolving 25 mg of sulfur in 10 mL of ODE in an ultrasonic bath. The ZnS shells were grown one layer at a time, by the successive injection of calculated amounts of zinc and sulfur solutions using a standard air-free procedure. The amount of precursors required was determined by estimated core size and shell lattice constant. The shell growth was performed at 210 °C, below the temperature for forming ZnS nanocrystals. The time interval between two successive injections was 20 min. Using this procedure, we have prepared CdSe/ZnS type I core−shell QDs with approximately 1−3 layers of shells. The actual CdSe core size and thicknesses of ZnS shells were determined by transmission electron microscopy (TEM). As shown in Figure S1, the size histograms can be fit by Gaussian functions with a center diameter and width of (2.74 nm, 0.59 nm), (3.26 nm, 0.60 nm), (3.78 nm, 0.91 nm), and (4.26 nm, 1.10 nm) for QDs with expected 0, 1, 2, and 3 monolayers (MLs) of ZnS shells, respectively. Based on the lattice constant of the wurzite ZnS (0.31 nm per monolayer), the average ZnS shell thicknesses (and layer number) for the three core/shell samples are 0.26 nm (0.8 ML), 0.52 nm (1.7 MLs), 0.76 nm (2.4MLs), respectively.

(34) Hines, M. A.; Guyot-Sionnest, P. *J. Phys. Chem.* **1996**, *100*, 468–71.
(35) Dabbousi, B. O.; RodriguezViejo, J.; Mikulec, F. V.; Heine, J. R.; Mattoussi, H.; Ober, R.; Jensen, K. F.; Bawendi, M. G. *J. Phys. Chem. B* **1997**, *101*, 9463–9475.
(36) Nazzal, A. Y.; Wang, X.; Qu, L.; Yu, W.; Wang, Y.; Peng, X.; Xiao, M. *J. Phys. Chem. B* **2004**, *108*, 5507–5515.
(37) Hagfeldt, A.; Gratzel, M. *Chem. Rev.* **1995**, *95*, 49–68.
(38) Cao, Y.; Rabinowitz, D. J.; Dixon, D. W.; Netzel, T. L. *Synth. Commun.* **2009**, *39*, 4230–4238.
(39) Maia, G.; Maschion, F.; Tanimoto, S.; Vaik, K.; Mäeorg, U.; Tammeveski, K. *J. Solid State Electrochem.* **2007**, *11*, 1411–1420.
(40) Burda, C.; Link, S.; Mohamed, M.; El-Sayed, M. *J. Phys. Chem. B* **2001**, *105*, 12286–12292.
(41) Burda, C.; Green, T. C.; Link, S.; El-Sayed, M. A. *J. Phys. Chem. B* **1999**, *103*, 1783–1788.
(42) Li, J. J.; Wang, Y. A.; Guo, W.; Keay, J. C.; Mishima, T. D.; Johnson, M. B.; Peng, X. *J. Am. Chem. Soc.* **2003**, *125*, 12567–12575.
(43) Yu, W. W.; Qu, L.; Guo, W.; Peng, X. *Chem. Mater.* **2003**, *15*, 2854–2860.

QD−AQ complexes were prepared by the addition of AQ to QD solutions in heptane, followed by sonication and filtration to remove undissolved AQ molecules. The ratio of adsorbed AQ to QD was controlled by varying the amount of added AQ and was determined by ultraviolet−visible (UV−vis) absorption spectroscopy. Because AQ is insoluble in heptane, all dissolved AQ is believed to be bound to the QD surface.

Femtosecond Transient Visible Absorption Measurements. The femtosecond (0.1 ps to 1 ns) transient absorption (TA) spectrometer used in this study is based on a regeneratively amplified Ti:sapphire laser system (coherent Legend, 800 nm, 150 fs, 3 mJ/pulse, and 1 kHz repetition rate). The pump pulse at 400 nm was generated by frequency doubling of the 800 nm pulse at a β-barium borate (BBO) crystal. The energy of the 400 nm pump pulse was controlled by a variable neutral-density filter wheel. The pump beam at the sample had a diameter of 300 μm. A white light continuum (WLC, from 410−690 nm) probe was generated by attenuating and focusing ~10 μJ of the 800 nm pulse into a rotating 2-mm-thick CaF_2 window. The probe beam was collimated and focused with Al parabolic reflectors onto samples with a beam size of 150 μm. After the sample, the probe beam was collimated and focused into a fiber-coupled spectrometer (Ocean Optics HR4000 Plus, 2048 pixel CCD, ~0.25 nm/pixel readout) and detected at a frequency of 10 Hz. The pump pulses were chopped by a synchronized chopper to the same frequency. During data collection, samples were constantly translated at a speed of 10 mm/min to avoid photodegradation. For all spectroscopy measurements, the samples were sealed in Harrick IR cells with a 400-μm-thick spacer sandwiched between two sapphire windows.

Nanosecond Transient Absorption Measurement. Nanosecond (0.5 ns to 50 μs) transient absorption was performed with the EOS spectrometer (Ultrafast Systems LLC). The pump pulses at 400 nm were generated in the regeneratively amplified Ti:sapphire laser system described above. The white light continuum probe pulse (380 to 1700 nm, 0.5 ns pulse width, 20 kHz repetition rate) was generated by focusing a Nd:YAG laser into a photonic cyrstal fiber. The probe pulses were synchronized with the femtosecond amplifier, and the delay time was controlled by a digital delay generator (CNT-90, Pendulum Instruments). The probe light was detected in fiber-optics coupled multichannel spectrometers with CMOS sensors. The nanosecond and femtosecond transient spectra overlap in delay times from 0.6−1 ns. To connect these spectra and kinetics, the nanosecond spectra have been scaled (to account for slight differences in excitation power densities) and shifted by 1.5 nm (to account for different calibrations of the spectrometers) such that the spectra at delay time 0.6−1 ns measured with femtosecond and nanosecond spectrometers agree with each other.

Results and Discussions

Characterization of QDs and QD−AQ Complexes. Figure 1a and b show the UV−vis absorption and photoluminescence (PL) spectra of QDs with the same CdSe core and 0, 0.8, 1.7, and 2.4 MLs of the ZnS shell. With increasing shell thicknesses, both the absorption and emission of the 1S exciton band are red-shifted due to the increased leakage of exciton wave function into the ZnS shell.[35] As shown in the Figure 1b inset, the ZnS coating suppresses the deep trap emission of the CdSe core and increases the quantum yield from 10% in the CdSe core to more than 40% in CdSe/ZnS (1.7 MLs) by passivating surface defects.[34,35] A further increase of the ZnS shell thickness leads to a reduction of the PL quantum yield, which can be attributed to an increase in the lattice-mismatch-induced defects.[35]

It was previously shown that the ET rate from QDs to adsorbed electron acceptors increases with the number of acceptors.[44] To quantify the influence of the ZnS shell thickness on the ET rate, it is essential to keep the same QD-to-AQ ratios for samples of different shell thicknesses. It has been shown

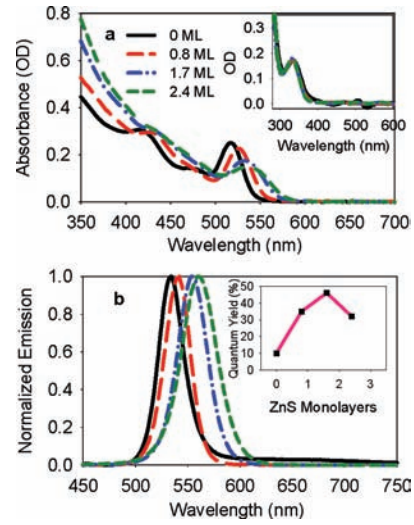

Figure 1. (a) UV−vis absorption and (b) normalized PL spectra of CdSe/ZnS QDs with 0 (black, solid), 0.8 (red, long-dash), 1.7 (blue, dash-dot), and 2.4 (green short-dash) MLs of ZnS in heptane solution. The integrated areas of the first exciton band are the same in these samples, indicating the same QD concentration. Inset in (a): Difference spectra between free QDs and QD−AQ samples of 0−2.4 MLs of ZnS, showing similar amounts of AQs in these samples. Inset in (b): The PL quantum yield as a function of the ZnS shell thickness.

previously that in type I CdSe/ZnS core/shell QDs, the oscillator strength of the 1S exciton transition is independent of the shell thickness in QDs of the same core size.[35] As shown in Figure 1, the four QD samples used in this study have the same integrated areas of the first exciton absorption band, indicating the same QD concentrations. The concentration of AQs in these samples can be determined from the UV−vis absorption spectra of AQ, which were obtained by subtracting the absorption of free QDs from that of QD−AQ complexes. As shown in the Figure 1a inset, these spectra show similar AQ absorptions for the band at ~330 nm, indicating similar QD-to-AQ ratios in these samples. Based on the measured absorbance and published extinction coefficient of AQ (ϵ_{330} = 4405 cm^{-1}/M)[45] and CdSe (ϵ_{517} = 164 456 cm^{-1}/M),[46] the average number of adsorbed AQ molecules per QD for these samples was estimated to be 3.5.

Exciton Dynamics in Free QDs. The femtosecond (0−1 ns) and nanosecond (1 ns−6 μs) transient absorption spectra of free QDs with different shell thicknesses are shown in Figure 2 (0.8 ML) and Figure S2 (0, 1.7, and 2.4 MLs). These spectra were obtained with low (14 nJ/pulse) 400 nm excitation to ensure that the average number of excitons per QD is much less than 1. The spectra show a long-lived bleach of exciton bands with a half-life of about 20 ns. TA signals in excited QDs can be attributed to two processes: state filling (SF) and a carrier induced stark effect (SE).[47,48] Due to the Pauli exclusion principle, the occupancy of a photoexcited electron in the lowest electron, lS(e), level reduces the transitions to this level by half, thus leading to the bleach of exciton bands in the transient difference spectra.[47] In addition to the SF features, electron−hole

(44) Boulesbaa, A.; Issac, A.; Stockwell, D.; Huang, Z.; Huang, J.; Guo, J.; Lian, T. *J. Am. Chem, Soc.* **2007**, *129*, 15132–15133.
(45) Du, H.; Fuh, R. A.; Li, J.; Corkan, A.; Lindsey, J. S. *Photochem. Photobiol.* **1998**, *68*, 141–142.
(46) Jasieniak, J.; Smith, L.; Embden, J. v.; Mulvaney, P.; Califano, M. *J. Phys. Chem. C* **2009**, *113*, 19468–19474.
(47) Klimov, V. I. *Annu. Rev. Phys. Chem.* **2007**, *58*, 635–673.
(48) Klimov, V. I.; McBranch, D. W. *Phys. Rev. B* **1997**, *55*, 13173–13179.

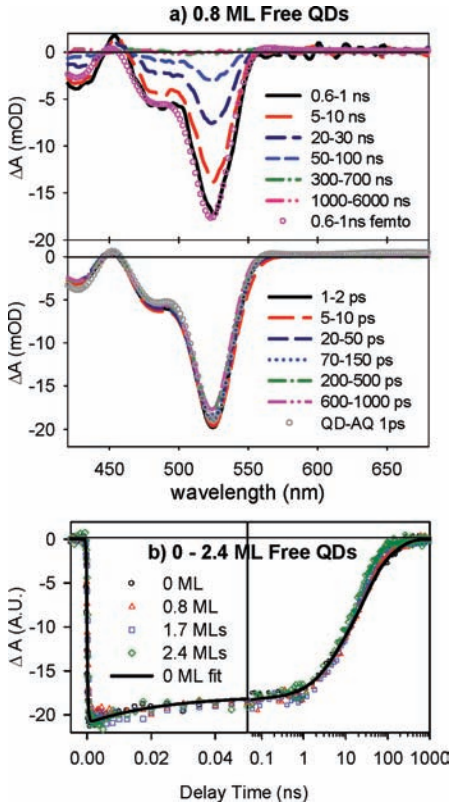

Figure 2. (a) Average visible TA spectra of free CdSe/ZnS(0.8 ML) QDs at indicated delay time windows after 400 nm excitation. Upper panel, 0.5 ns−6 μs; lower panel, 1 ps−1 ns. The TA spectrum at 0.6−1 ns (open pink circles) from the lower panel has been reproduced in the upper panel to show good agreement between the spectra recorded using femtosecond and nanosecond TA spectrometers. Also shown in the lower panel is the average TA spectrum of QD−AQ complexes at ∼1 ps (gray open circles), which agrees well with that of free QDs. (b) Comparison of 1S exciton bleach recovery kinetics in CdSe QDs with 0, 0.8, 1.7, and 2.4 MLs of ZnS shells. The solid line is a fit to the bleach recovery of the CdSe core only QDs. The horizontal axis is in linear scale in the left panel (0−50 ps) and in logarithmic scale in the right panel (50 ps−1 ns).

pairs can generate a local dc electrical field, which shifts the excitonic bands to a longer wavelength due to the dc Stark effect, and leads to derivative-like features in the difference spectra.[49,50] The amplitude of the shift has been predicted to depend on the nature of the trapped carriers and the size of the QDs.[50] As shown in Figures 2 and S2, the amplitude of the SF bleach signal is much larger than that of SE signal in free QDs. Therefore the 1S exciton bleach recovery time provides a direct probe of the lifetime of 1S electrons in free QDs.[47,51] For all QDs with different shell thicknesses, the bleach recovers by <15% within 1 ns. It confirms that under our experimental conditions most excited QDs have 1 exciton and the effect of exciton−exciton annihilation, which occurs on the tens to hundreds of picoseconds time scale, can be neglected.[52,53] For these QDs, excitation at 400 nm promotes an electron above the 1P(e) level, which relaxes to the 1S(e) level to give rise to the bleach in the 1S exciton transition. A fit of the 1S bleach formation kinetics reveals a rise time of ∼330 fs, consistent with the reported 1P−1S electron cooling time in related QDs.[47,54,55] The fitting parameters for the bleach recovery kinetics are listed in Table S1.

Charge Transfer Dynamics in QD−AQ Complexes. Visible TA spectra of QD−AQ samples with different shell thicknesses are shown in Figure 3 (0.8 and 2.4 MLs) and Figure S3 (0 and 1.7 MLs). Femtosecond TA spectra (0.1 ps to 1 ns, lower panel) were acquired under the same conditions as those for free QDs to ensure negligible multiexciton decay in the bleach kinetics. The nanosecond TA spectra (from 0.5 ns to 6 μs) were also recorded under a similar excitation power density as that for the femtosecond measurement. In addition to amplitude changes, the TA spectra of QD−AQ complexes show noticeable changes of spectral shapes and clear red shifts of the peak of the bleach band with increasing delay times between 1 ps and 1 ns. The red shift becomes more pronounced with increasing shell thicknesses. At delay times < 1 ps, the TA spectra are dominated by the bleach signals arising from state filling. These spectral features (designated as $A_{QD^*}(\lambda)$) are identical to those in free QDs and their spectral shape is time-independent, as shown in Figures 2 and S2. Therefore its amplitude, $N_{QD^*}(t)$, reflects the population of excited QDs. At longer delay times (>1 ns) the transient spectra show derivative-like features caused by the stark effect induced shift of exciton bands,[49] and a broad absorption band centered around 650 nm. This absorption band can be more clearly seen in the nanosecond TA spectra (upper panels of Figure 3), in which the probe wavelength is extended to 750 nm. This feature can be assigned to the one-electron reduced AQ radical, which has been reported to show an absorption band at ∼600 nm.[41,56,57] Furthermore, the amplitude of the exciton bleach at 1 ns is much smaller than its initial value at ∼1 ps, suggesting the decrease of the 1S electron population. All these features suggest the transfer of electrons from the 1S(e) level in the excited QDs to the AQ molecules (to form AQ^-) between 1 ps and 1 ns, as described by the first step in eq 1. From 1 ns to 6 μs, the shape of the transient spectra remains unchanged, as indicated by clear isosbestic points shown in Figure 3. These spectra, denoted as $A_{CS}(\lambda)$, can be attributed to the charge separated state ($QD-AQ^-$). The decrease of the amplitude, $N_{CS}(t)$, of this spectral signature from 1 ns to 6 μs can be attributed to the charge recombination process, i.e. back ET from AQ^- to the oxidized QD, to regenerate the AQ and QD in their ground states, as described by the second step in eq 1.

In the intermediate delay times between ∼1 ps and ∼1 ns, the transfer of electrons from the 1S(e) level to the adsorbed AQ reduces the population of excited QDs and increases the population of the charge separated state, leading to the time-dependent red-shift of the observed TA spectra. Because of the overlap of the signals of the QD excited state and charge separated state in the exciton bleach region, these contributions have to be separated to obtain the QD excited state decay kinetics. To do so, we fit the transient spectra ($S(\lambda,t)$) in Figure

(49) Norris, D. J.; Sacra, A.; Murray, C. B.; Bawendi, M. G. *Phys. Rev. Lett.* **1994**, *72*, 2612–2615.
(50) Wang, Y.; Suna, A.; McHugh, J.; Hilinski, E. F.; Lucas, P. A.; Johnson, R. D. *J. Chem. Phys.* **1990**, *92*, 6927–6939.
(51) Huang, J.; Stockwell, D.; Huang, Z.; Mohler, D. L.; Lian, T. *J. Am. Chem. Soc.* **2008**, *130*, 5632–5633.
(52) Nozik, A. J. *Annu. Rev. Phys. Chem.* **2001**, *52*, 193–231.
(53) Klimov, V. I.; Mikhailovsky, A. A.; McBranch, D. W.; Leatherdale, C. A.; Bawendi, M. G. *Science* **2000**, *287*, 1011–1013.
(54) Huang, J.; Huang, Z.; Yang, Y.; Zhu, H.; Lian, T. *J. Am. Chem. Soc.* **2010**, *132*, 4858–4864.
(55) Cooney, R. R.; Sewall, S. L.; Dias, E. A.; Sagar, D. M.; Anderson, K. E. H.; Kambhampati, P. *Phys. Rev. B* **2007**, *75*, 245311/1–245311/14.
(56) Levin, P. P.; Costa, S. M. B.; Ferreira, L. F. V. *J. Phys. Chem.* **1995**, *99*, 1267–1275.
(57) Okamoto, K.; Hasobe, T.; Tkachenko, N. V.; Lemmetyinen, H.; Kamat, P. V.; Fukuzumi, S. *J. Phys. Chem. A* **2005**, *109*, 4662–4670.

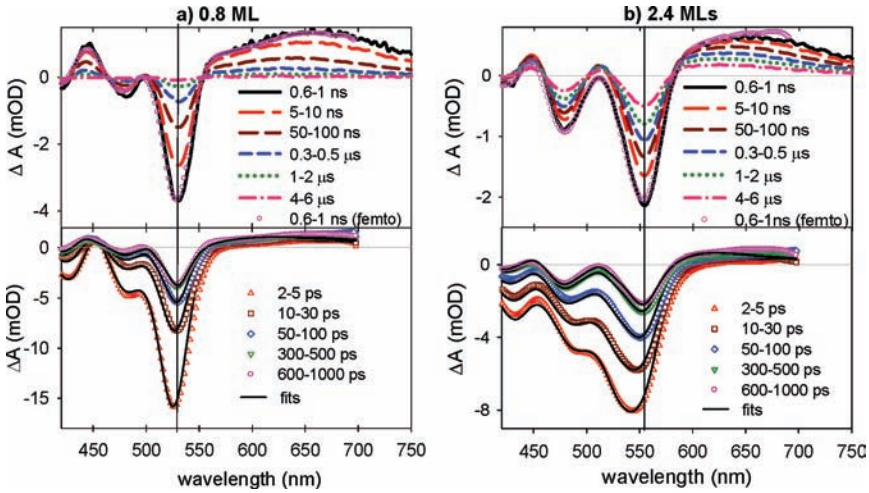

Figure 3. Average visible TA spectra of QD−AQ with (a) 0.8 ML of ZnS and (b) 2.4 MLs of ZnS at indicated delay time windows (0−1 ns, lower panels; 0.5 ns−6 μs, upper panels) after 400 nm excitation. The vertical scale in the upper panels has been expanded to more clearly show the anion features. Solid lines in the lower panel are fits to the data (symbols) according to eq 3 in the text. The TA spectrum at 600−1000 ps (circles) from the lower panel has been reproduced in the upper panel to show good agreement between the spectra recorded using femtosecond and nanosecond TA spectrometers.

3 and S3 by the sum of the TA spectra of the excited QDs and charge-separated state according to eq 3:

$$S(\lambda, t) = N_{QD^*}(t) \cdot A_{QD^*}(\lambda) + N_{CS}(t) \cdot A_{CS}(\lambda) \qquad (3)$$

$N_{CS}(t)$ and $N_{QD^*}(t)$ are the only variable parameters used in the fit. The fitted averaged spectra at indicated delay time windows between ~1 ps and 1 ns are shown in Figures 3 and S3. It is clear that the TA spectra can be well reproduced by the sum of the base spectra for the excited QD and charge-separated state with time-dependent populations, supporting the spectral assignment discussed above. $N_{CS}(t)$ is set to zero at $t < 1$ ps and is assumed to be proportional to the amplitude of the transient spectra at $t > 1$ ns. The value of $N_{QD^*}(t)$ is set to be proportional to the 1S exciton bleach amplitude before 1 ps.

The kinetics of $N_{QD^*}(t)$ and $N_{CS}(t)$ obtained from the fit as well as the anion ($N_{AQ^-}(t)$) are compared in Figure 4 (0 and 0.8 ML) and Figure S4 (1.7 and 2.4 MLs). The anion kinetics ($N_{AQ^-}(t)$) was obtained by averaging the transient signal at 640−660 nm. Because $N_{CS}(t)$ and $N_{AQ^-}(t)$ both reflect the population of the charge separated states, their kinetics should agree with each other. As shown in Figures 4 and S4, these kinetics agree well with each other, validating our spectral fitting procedure. Furthermore, we have normalized their amplitudes such that they agree with $(1 - N_{QD^*}(t))$. The latter reflects the population change of the excited QDs, which should be equal to $N_{CS}(t)$ and $N_{AQ^-}(t)$ when there is negligible charge recombination. As shown in Figures 4 and S4, within the first T_1 ps ($T_1 \approx 10$ ps, 300 ps, 500 ps, and 1 ns for QDs with 0, 0.8, 1.7, and 2.4 MLs of shells, respectively), $(1 - N_{QD^*}(t))$ agrees with $N_{CS}(t)$. At $t > T_1$, the $N_{CS}(t)$ and $N_{AQ^-}(t)$ start to decrease, deviating from $(1 - N_{QD^*}(t))$ and indicating the onset of the charge recombination process.

Shell Thickness Dependent Charge Separation and Recombination Kinetics. The kinetics of the excited QD population ($N_{QD^*}(t)$) and anion population ($N_{AQ^-}(t)$) for the QD−AQ complexes with different shell thicknesses are compared in Figure 5. It is clear that with the increasing ZnS shell thickness, both the QD excited state and anion decay become slower, suggesting the decrease of the rates of both the charge separation from the QD to AQ and the subsequent charge recombination process.

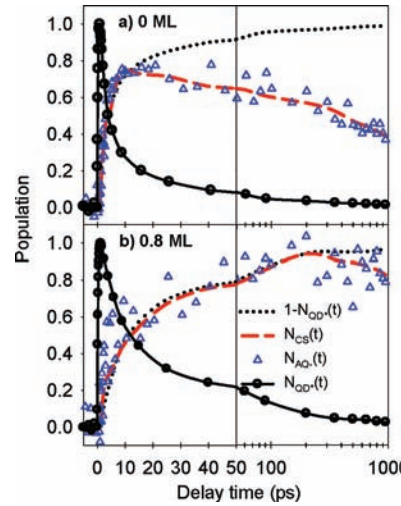

Figure 4. Comparison of the kinetics of QD excited state ($N_{QD^*}(t)$, open black circles), charge separated state ($N_{CS}(t)$, red lines), and anion ($N_{AQ^-}(t)$, open blue triangles) of QD−AQ complexes with (a) 0 and (b) 0.8 MLs of ZnS shells. $N_{QD^*}(t)$ and $N_{CS}(t)$ are obtained from fitting the transient data according eq 3. $N_{AQ^-}(t)$ is the TA signal at 640−660 nm. Also shown as the dotted lines is $(1 - N_{QD^*}(t))$. Both $N_{CS}(t)$ and $N_{AQ^-}(t)$ have been scaled such that their formation kinetics agree with $(1 - N_{QD^*}(t))$.

The charge separation and recombination kinetics are not single-exponential. As shown in Figure 5a, the kinetics of the QD excited state can be fit according to the following equation:

$$N_{QD^*}(t) = \sum_i A_i e^{-k_{CS,i}t} - e^{-k_0 t} \qquad (4)$$

Here, $1/k_0$ (~330 fs) is the formation time of the 1S exciton bleach. This rise time reflects the cooling of the conduction band electrons to the 1S(e) level, similar to those in the free QDs. Satisfactory fits to the QD decay kinetics can be obtained using triexponential functions with amplitudes and time constants of A_i *and* $k_{CS,i}$, respectively. The fitting parameters are listed in Table S2.

According to eq 1, the population of the charge separated state increases with the rate of the charge separation process and decays with the rate of charge recombination. The anion kinetics traces can be fit to eq 5:

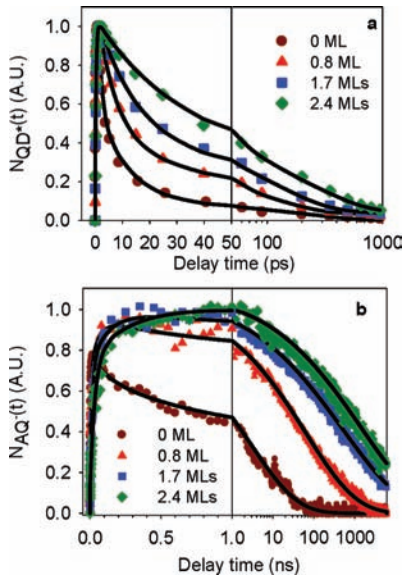

Figure 5. Comparison of QD excited state (a) and anion (b) population kinetics in QD−AQ samples of different ZnS shell thicknesses. The rates of charge separation and recombination, which are determined from the decay of excited state and anion populations, respectively, decrease with increasing shell thickness. Black lines are fits of the charge separation and recombination kinetics according to eqs 4 and 5, respectively. The delay time in (a) is in linear scale for 0−50 ps (left) and logarithmic scale for 50−1000 ps (right). The delay time in (b) is in linear scale for 0−1 ns (left) and logarithmic scale for 1− 6000 ns (right).

$$N_{AQ^-}(t) = \sum_i A_i e^{-k_{CS,i}t} - e^{-(t/\tau_R)^\alpha} \qquad (5)$$

The parameters for charge separation have been determined by fitting the decay of the QD excited state as discussed above. The decay of the charge separated state can be best fit by stretched exponential functions, as shown in Figure 5b, although they can also be fit by triexponential functions. The characteristic times τ_R and exponents α of the best stretched exponential fits are listed in Table S3.

Both the charge separation and recombination rates are highly heterogeneous, similar to those observed previously for QD- or dye-sensitized TiO_2 nanoparticles.[58−61] The heterogeneity can be caused by the distributions of the number of adsorbates on each QD,[62] adsorption sites, and adsorbate conformations, as well as the QD core size and shell thickness. We use the half-life time for the QD excited state and anion decay to represent the average charge separation and recombination times. The charge separation (and recombination) half-life times are 3.4 ps (0.75 ns), 10.5 ps (30 ns), 23.6 ps (230 ns), and 45.0 ps (800 ns) for QDs with 0, 0.8, 1.7, and 2.4 MLs of shells, respectively. Plots of the logarithm of the charge separation and recombination rates (the inverse of half-life times) as a function of shell thickness yield straight lines, as shown in Figure 6. It suggests that both the charge separation and recombination rates decay

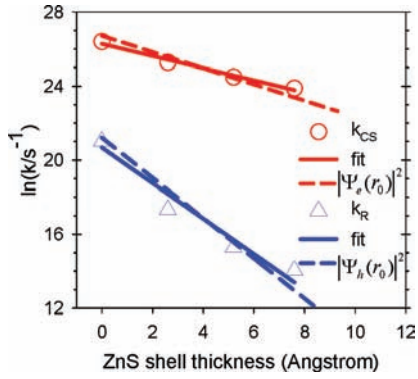

Figure 6. Plot of the logarithm of charge separation (red circles) and recombination (blue triangles) rates as a function of the ZnS shell thickness. These rates are determined from the half-lives of the QD excited state and anion decays, respectively. Best fits (red and blue solid lines) of the data according to eq 2 yield slopes ($-\beta$) of −0.35 (±0.03) and −0.91 (±0.14) Å^{-1} for charge separation and recombination rates, respectively. Also shown are the calculated electron (red dashed line) and hole (blue dashed line) densities at the shell surface as a function of shell thickness. For better comparison, the electron (hole) densities for the bare QDs were normalized to the measured charge separation (recombination) rates.

exponentially with the shell thickness. Fitting the thickness dependence to eq 2 yields a slope β of 0.35 ± 0.03 and 0.91 ± 0.14 Å^{-1} for charge separation and recombination rates, respectively. We have also determined average charge separation and recombination rates from amplitude-weighted average time constants (obtained by three exponential fits) and characteristic stretch exponential time constants. As shown in Figure S6, although the average rates determined by these approaches vary, the slopes of their dependence on the shell thickness (β) remain the same.

The rate of nonadiabatic electron transfer processes is given by[63]

$$k_{ET}(d) = \frac{2\pi}{\hbar}\frac{|H(d)|^2}{\sqrt{4\pi\lambda k_B T}} \exp\left[-\frac{(\lambda + \Delta G(d))^2}{4\lambda k_B T}\right] \qquad (6)$$

where ΔG is the driving force, H the electronic coupling strength, and λ the total reorganization energy. The reorganization energy for ET from QDs can be assumed to be negligible because of the delocalized 1S wave function. Thus the total reorganization energy is controlled by that of the molecule and should remain unchanged for QDs with different shell thicknesses. In this system, the 1P−1S electron relaxation (~330 fs) is much faster than ET (>3.4 ps), suggesting that ET occurs from the 1S electron level. This is confirmed by the agreement between the kinetics traces of the 1S exciton bleach recovery and the AQ^- formation shown in Figures 4 and S4. As an initial model for the exciton dissociation process, we assume that the transfer of the electron is uncoupled with the hole dynamics. With this assumption, the electronic coupling strength H for the charge separation process depends on the overlap of the 1S electron wave function with the lowest unoccupied molecular orbital (LUMO) in AQ, and its driving force (ΔG_{CS}) is given by the Gibbs free energy changes for AQ reduction and QD excited state oxidation ($\Delta G_{CS} = -e[V_{AQ/AQ^-} - V_{QD^+/QD^*}]$). Here, V_{X/X^-} denotes the standard redox potential of the X/X^- couple. For the recombination process, H depends on the overlap of the highest occupied molecular orbital of the AQ radical anion

(58) Anderson, N. A.; Lian, T. *Annu. Rev. Phys. Chem.* **2005**, *56*, 491–519.
(59) Asbury, J. B.; Anderson, N. A.; Hao, E.; Lian, T. *J. Phys. Chem. B* **2003**, *107*, 7376–7386.
(60) Haque, S. A.; Tachibana, Y.; Willis, R. L.; Moser, J. E.; Graetzel, M.; Klug, D. R.; Durrant, J. R. *J. Phys. Chem. B* **2000**, *104*, 538–547.
(61) Tachibana, Y.; Umekita, K.; Otsuka, Y.; Kuwabata, S. *J. Phys. Chem. C* **2009**, *113*, 6852–6858.
(62) Boulesbaa, A.; Huang, Z.; Wu, D.; Lian, T. *J. Phys. Chem. C* **2010**, *114*, 962–969.
(63) Marcus, R. A.; Sutin, N. *Biochem. Biophys. Acta* **1985**, *811*, 265–322.

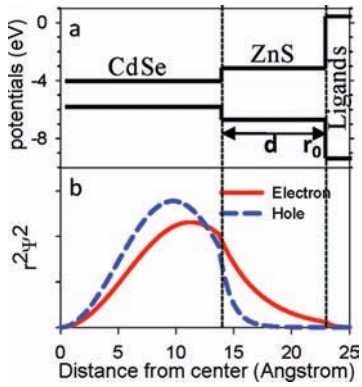

Figure 7. (a) Band alignments and (b) radial distribution functions for 1S electron and hole levels of CdSe/ZnS core/shell QD with a 13.7 Å CdSe core and 3 monolayers of ZnS shell (thickness *d*). Vertical dashed lines indicate CdSe/ZnS and ZnS/organic ligand interfaces. r_0 indicates the distance from the outer surface of the ZnS shell to the center of the QD. Potentials are relative to the vacuum energy level.

(which corresponds to the LUMO of AQ) with the hole wave function in the valence band of the QDs and the ET driving force (ΔG_R) is determined by the Gibbs free energy changes for QD^+ reduction and AQ radical anion oxidation ($\Delta G_R = -e[V_{QD^+/QD} - V_{AQ/AQ^-}]$). Both the driving force and the coupling strength can vary with the shell thickness.

To quantify the effect of ZnS shell thickness on the electron (hole) transfer rate, we calculate the eigen function and energy of the electrons and holes in CdSe/ZnS type I QDs by modeling them as particles confined in spherical wells of finite depth.[35,64] The effective masses of electrons (holes) are $m_e^* = 0.13$ ($m_h^* = 0.45$) in CdSe and 0.25 (1.3) in ZnS.[65] The conduction and valence band edge positions are −4.0 and −5.7 V in the CdSe core, −3.1 and −6.6 V in the ZnS shell, and 0 and −8.4 eV in the surrounding organic medium, as shown in Figure 7a.[65,66] The Schrodinger equation of the system is solved numerically to obtain the wave function and energy of the lowest (1S) electron and hole levels.[35] The Coulomb interaction between the electron and hole is treated as a first-order perturbation (the dielectric constants are $\varepsilon = 10\varepsilon_0$ in CdSe and $8.9\varepsilon_0$ in ZnS), from which the energy of the first exciton state can be calculated.[67] The reported conduction band edge position of bulk CdSe crystals varies considerably, ranging from −4.0 to −3.5 vs the vacuum level.[68] This uncertainty affects the calculated values of electron and hole energy levels. The values reported here (using a conduction band edge of −4.0 V) represent their lower limits. However, this uncertainty in absolute band edge position has negligible effect on the shell thickness dependence of the energy and wave function to be discussed below.

The calculations were performed for QDs with the same core and 0, 1, 2, and 3 monolayer(s) of ZnS shells. The core diameter was chosen to be 2.74 nm, which is the average diameter of CdSe core only QDs determined by TEM (Figure S1). The calculated first exciton peaks for these QDs and their shell thickness dependence are in reasonable agreement with the measured absorption spectra, as shown in Figure S5. For example, the calculated and measured first exciton peak positions in CdSe core only QDs are 513 and 517 nm, respectively. The calculated 1S exciton energy decreases by 100 meV for QDs with 0 to 3 MLs of ZnS shells. This value agrees well with the measured value of ∼80 meV. From the energies of the 1S electron, hole, and exciton, the redox potentials for QD 1S excited state oxidation (V_{QD^+/QD^*}), 1S excited state reduction (V_{QD^*/QD^-}), and ground state oxidation ($V_{QD^+/QD}$) can be calculated.[10,69] The calculated values for (V_{QD^+/QD^*}, V_{QD^*/QD^-}, $V_{QD^+/QD}$) are (−0.87, +1.73, +1.55) and (−0.86, +1.63, +1.46, V NHE) for QDs with 0 and 3 MLs of ZnS shells, respectively. Using a reduction potential of −0.70 V vs NHE for AQ and the calculated V_{QD^+/QD^*}, the driving force for the charge separation process can be estimated to be larger (more negative) than −0.17 V and changes negligibly with the shell thickness (<10 meV). The driving force for the charge recombination process is estimated to be −2.25 V and decreases by <90 meV from core only QDs to those with 3 MLs of shells. It is clear that the energetic changes cannot account for the observed shell thickness dependent ET rates. It suggests that the shell thickness dependence is caused by the variation of the electronic coupling strength for ET.

Figure 7b shows the radial distribution functions of the 1S electron and hole in QDs with 3 MLs of ZnS shells. Both the electron and hole wave functions spread into the ZnS layer, and their amplitudes decay exponentially with the shell thickness. The electronic coupling strength for charge separation (recombination) should depend on the overlap integrals of the electron (hole) wave function with the LUMO of AQ. Because the AQ molecules likely bind on the outermost layer of the inorganic surface (CdSe surface in bare QDs and ZnS surface in core/shell QDs) by displacing the organic ligands or occupying uncoordinated sites, we assume that the coupling strength is proportional to the amplitude of the electron (hole) wave function $\Psi(r_0)$ at the QD/organic ligand interface. According to eq 6, the electron transfer rate should be proportional to the square modulus of the coupling strength: $k_{ET} \propto |\Psi(r_0)|^2$. Under these assumptions, the calculated relative electron (hole) density on the QD surface can be used to determine the relative electron (hole) transfer rate. As shown in Figure 6, the electron (hole) density has been scaled such that the values on the bare CdSe QDs (without shell) match their charge separation (recombination) rate. The calculated surface electron and hole densities decay exponentially with ZnS layer thickness with exponential decay factors of 0.43 $Å^{-1}$ for the electron and 1.09 $Å^{-1}$ for the hole, which are in reasonable agreement with the measured thickness dependence of the average charge separation and recombination rates. This agreement confirms that, in CdSe/ZnS type I QDs, the ZnS shell serves as a tunneling barrier for the electron and hole transfer and slows down their rates by decreasing the electronic coupling with the adsorbate. A similar exponential dependence of ET rate with the thickness of the insulating spacer has been extensively studied in molecular systems and in dye-sensitized oxide nanoparticles.[70−73] Although the calculation is for the 1S hole level, the dependence on shell thickness should be similar for the trapped hole, because

(64) Haus, J. W.; Zhou, H. S.; Honma, I.; Komiyama, H. *Phys. Rev. B* **1993**, *47*, 1359.
(65) Berger, L. I. *Semiconductor Materials*; CRC Press: 1997.
(66) Salomon, A.; Boecking, T.; Seitz, O.; Markus, T.; Amy, F.; Chan, C.; Zhao, W.; Cahen, D.; Kahn, A. *Adv. Mater.* **2007**, *19*, 445–450.
(67) Sze, S. M. *Modern Semiconductor Device Physics*; John Wiley: New York, 1998.
(68) *Semiconductor Electrodes*; Finklea, H. O., Ed.; Elsevier: New York, 1988; Vol. 55.
(69) Brus, L. *J. Chem. Phys.* **1983**, *79*, 5566–5571.
(70) Lewis, F. D.; Wu, T.; Zhang, Y.; Letsinger, R. L.; Greenfield, S. R.; Wasielewski, M. R. *Science* **1997**, *277*, 673–676.
(71) Guo, J.; She, C.; Lian, T. *J. Phys. Chem. C* **2007**, *111*, 8979–8987.
(72) Newton, M. D. *Chem. Rev.* **1991**, *91*, 767–792.
(73) Anderson, N. A.; Ai, X.; Chen, D.; Mohler, D. L.; Lian, T. *J. Phys. Chem. B* **2003**, *107*, 14231–14239.

the shell acts as a tunneling barrier. Unfortunately, it is not clear whether the charge recombination occurs via the 1S or trapped hole because of the lack of clear spectral signatures for the hole in our experiment.

It is interesting to note that, with increasing shell thicknesses, the charge recombination rate decays much faster than the charge separation rate. With 2.4 MLs of ZnS shells, the measured charge separation rate decreases by a factor of 15, whereas the recombination rate is reduced by 1000-fold. According to the model calculation described above, this difference can be attributed to the larger effective mass of the hole compared to the electron in the ZnS shell. Considering the fast charge separation rate (∼3.4 ps) in CdSe−AQ complexes and the long intrinsic exciton lifetimes of these QDs (∼20 ns), it is possible to maintain a high charge separation yield while greatly prolonging the lifetime of the charge separated state by increasing the shell thickness. In fact, for QD−AQ, both the peak population and lifetime of the charge separated state increases with the shell thickness because of the retardation of the charge recombination process (see Figure 5). The highest percentage of the charge separated state population (near unity at its peak) and the longest charge separation lifetime (half-life of ∼0.8 μs) were achieved with the largest shell thickness (2.4 MLs of ZnS) examined in this study. Thus, by tuning the shell thickness and changing the shell materials in type I QDs, it is possible to design more efficient and stable QD-based photovoltaic devices.

Conclusion

In summary, we have investigated how the shell thickness affects the charge separation and recombination kinetics of CdSe/ZnS type I core/shell QDs. We have demonstrated that the excitons in the QDs can be dissociated by electron transfer to the adsorbed AQ, which is followed by charge recombination on a much slower time scale. For core only CdSe QDs, the half-life times for charge separation and recombination are 3.4 ps and 0.75 ns, respectively. With the increasing shell thickness, both the charge separation and recombination rates decrease exponentially with exponential factors of 0.35 ± 0.03 and 0.91 ± 0.14 Å^{-1}, respectively. Model calculations of these core/shell QDs show that the trends in charge separation and recombination rates agree well with the exponential decreases of the electron and hole densities at the QD surface with the shell thickness. The faster exponential decay of the recombination rate with the shell thickness can be attributed to the steeper decrease of the surface hole density, which is caused by the larger hole effective mass (compared to the electron) in the ZnS shell. The results of this study suggest possible ways of optimizing the charge separation yield and lifetime by controlling the thickness and nature of the shell materials, achieving more efficient and stable QD-based solar cells.

Acknowledgment. The work was supported by the National Science Foundation (CHE-0848556) and Petroleum Research Fund (PRF#49286-ND6). The anthroquinone used in this study was a generous gift from the late Professor Thomas L. Netzel of Georgia State University.

Supporting Information Available: TEM images, transient absorption spectra of QDs and QD−AQ complexes, calculated 1S exciton peak positions, and tables of fitting parameters. This material is available free of charge via the Internet at http://pubs.acs.org.

JA106710M